FLUCOME 2009
10th International Conference on Fluid Control, Measurements, and Visualization
August 17–21, 2009, Moscow, Russia

COMPUTATIONAL STUDY OF THE SEPARATED FLOW STRUCTURE INDUCED BY THE SYNTHETIC JET ON A BACKWARD-FACING STEP

Koichi Okada[1], Kozo Fujii[2] and Koji Miyaji[3]

ABSTRACT

In order to clarify the mechanism of the synthetic jet on the massively separated flow appearing at the backward-facing step, flow-fields with/without the synthetic jet are numerically simulated. Implicit large eddy simulation using high-order and high-resolution compact difference scheme is applied. A flow field without a synthetic jet, flow fields with the synthetic jet at non-dimensional frequencies of the wall oscillation, F^+_h =0.2 and F^+_h=2.0, are computed, where no-dimensional frequency of F^+_h is normalized with the height of backward-facing step and free stream velocity. Although previous studies show that each F^+_h is good conditions, the present computation shows that length of the separation region only at F^+_h =0.2 become 25 percent shorter than that without synthetic jet. It seems that F^+_h =0.2 is near shear layer instability frequency without the synthetic jet. Strong two-dimensional vortices induced from the synthetic jet interact with the shear layer, which results in the increase of the Reynolds stress. At F^+_h =2.0, length of the separation region is almost same as that without synthetic jet. Mixing is not enhanced in the shear layer because Reynolds stress does not increase. Weak and short periodic vortices induced from the synthetic jet do not interacts with the shear layer very much.

Keywords: Active flow control, Backward-facing step, CFD, Separation flow, Synthetic jet

INTRODUCTION

Flow-control technology has been widely researched to improve the aerodynamic performance of transportation systems such as aircrafts and cars. The common objectives in many cases are to prevent massive flow separations for both the external and internal flows. Passive flow control devices such as a vortex generator and natural bleed have been mainly used for practical applications because of its simplicity and lightweight, while an active flow control using continuous blowing and suction has been also investigated (Okada and Hiraoka, 2003) due to rather large effects on the main stream. The drawbacks of such large jets are the complex duct systems and heavyweights. Therefore, in recent years, many researchers have been studying active flow control methods based on micro scale devises. One of them is a “synthetic jet”. A typical synthetic jet induces vortices at an orifice exit by oscillating the wall at

[1] Corresponding author: Yokohama National University, Department of Ocean and Space Engineering, e-mail: okada@flab.isas.jaxa.jp

[2] Japan Aerospace Exploration Agency, Institute of Space and Astronautical Science e-mail: fujii@flab.isas.jaxa.jp

[3] Yokohama National University, Department of Ocean and Space Engineering, e-mail: miyaji-k@ynu.ac.jp

the bottom of the cavity connected to the orifice (Fig. 1). The synthetic jet has advantages over conventional flow control devises such as active flow control capability, light weight and compactness because it does not require any air-supplier systems and the total mass flow of the jet is zero. It is suitable for many kinds of airplanes including UAVs/MAVs and helicopters. Dynamic control capability is favorable, too.

Most of previous experimental studies on the synthetic jet have been focused on demonstrating effects of the synthetic jet for flow control, or finding optimal conditions for the synthetic jet on an airfoil or backward facing step. In experimental studies, Amitay *et al.* (2001) and Seifert and Darabi (1996) parametrically studied in their experiments the effects of the position of installation, non-dimensional jet frequency (based on chord length or separation length and free stream velocity), and the jet mass flow on the flow separation control around an airfoil. Glezer *et al.* (2005) researched especially non-dimensional jet frequency effects on the flow separation control around an airfoil. Previous research (Seifert; Darabi, 1996) showed that good non-dimensional jet frequency is 1(O) but they showed better non-dimensional jet frequency is 10(O). On the other hand, Yoshioka *et al.* (2001) studied experimentally separation control of backward-facing step configuration using periodic excitation and showed that better no-dimensional frequency F^+_h (based on height of backward-facing step and free stream velocity) is 0.2. Vukasinovic *et al.* (2004) studied experimentally separation control of backward-facing step configuration using synthetic jet and showed that F^+_h=10(O) is effective value. However, the flow control mechanism of the synthetic jet has not been clear yet.

As for numerical studies, Kral *et al.* (1998) compared synthetic jet and steady jet results on the flow separation control around an airfoil and show effectiveness of synthetic jet using two-dimensional RANS computation but flow control mechanism has not been clear yet. Kral *et al.* (1997) compared computed and experimental results and found that flow computation with top-hat type velocity boundary condition agrees with experimental time-mean vertical velocity in quiescent condition. Mittal *et al.* (2001) has computationally shown that the orifice exit velocity in quiescent condition is different from that in the condition with external flow. Most of previous simulations do not consider effect of cavity flow on separation control.

Therefore, it is necessary to research the optimal usage on flow control for improving performance and efficiency drastically. The objective of the present study is to understand mechanics of separation flow control. The synthetic jet in static air condition was analyzed as our preliminary study (Okada *et al.*, 2008). The objective of the study was to investigate effect of internal flows in synthetic jet cavity. First, three-dimensional computation solving both the orifice jet and internal flow in the cavity are compared with conventional simulation approaches. 3D vortex structure is captured in the cavity model. Then, the effects of dimensional parameters are researched to understand the flow induced by the synthetic jet. Different frequency cases change three-dimensional flow fields. Different amplitude cases, changes three-dimensional flow fields and vortex intensity.

Research with external flow is conducted as next step. A backward-facing step configuration is chosen for the first step of line of this research, because the flow field and geometry become simpler than those around an airfoil. In order to clarify the mechanism of the synthetic jet on the massively separated flow appearing at the backward-facing step, flow-fields with/without the synthetic jet are numerically simulated. The present analysis is focused on the frequency characteristics of the synthetic jet.

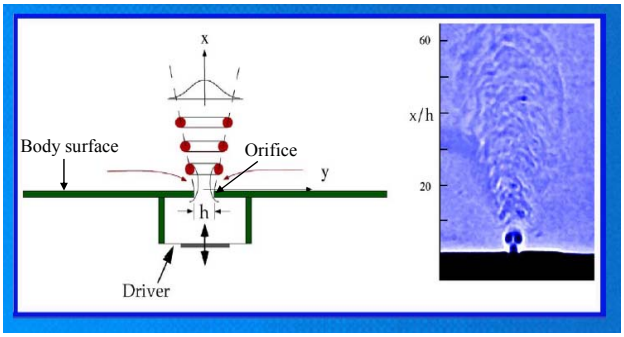

Fig. 1. Synthetic jet (Mallinson, 1999)

ANALYSIS MODELS

A. Configuration of synthetic jet

A geometric configuration of the synthetic jet in the reference (Rizzetta and Visbal, 1999) is chosen in this study (Fig. 2). The non-dimensional orifice depth d is equal to the non-dimensional orifice width h. The cavity depth Z_D is $10d$ and the cavity width X_L is $15d$. The cavity span length in the y direction is treated to have infinite length in the simulation since this study target two-dimensional configuration.

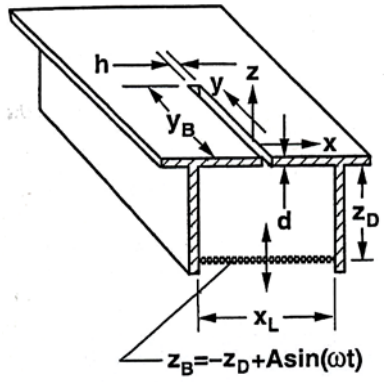

Fig. 2. Synthetic jet configuration

B. Modeling of the wall oscillation

The oscillation of the cavity wall is defined by equation (1).

$$h_w(x,t) = A \cdot \sin(2\pi F^+_h t) \tag{1}$$

Here, amplitude of the wall oscillation A is constant value. F^+_h is no-dimensional frequency of the wall oscillation. Input parameter value show at computational conditions.

C. Configuration of Backward-facing step

The backward-facing step configuration and flow conditions are same of Jovic's study (1996) because this experiment has various comparable data for validation of No-control case. Fig. 2 show whole image of the experiment. Unit is centimeter and the scale of this figure is not collect. Blue region is the computational region.

D. Numerical method

Three-dimensional compressible Navier-Stokes equations are employed as the governing equations. These equations are solved in the generalized curvilinear coordinates. The spatial derivatives of convective terms and viscous terms, metrics, and Jacobian are evaluated by the sixth-order compact difference scheme (Lele, 1992) since an induced velocity by synthetic jet are very small and the boundary layer is efficiently solved. Near the boundary, second-order explicit difference schemes are used. The tenth-order filtering (Gaitonde and Visbal, 2000) is used with filtering coefficient of 0.45. Visbal and Gordnier's approach (Visbal and Gordnier, 2000) for computation of metrics and Jacobian on deforming and moving meshes is used for satisfying the computation the geometric conservation law. For time integration, regarding the characteristic of the computer, a kind of implicit method Lower-Upper Symmetric Alternating Direction Implicit and Symmetric Gauss-Seidel (ADI-SGS) is used for time integration. This algorithm uses same kind of idea of Four-Factored Symmetric Gauss-Seidel (FF-SGS) (Fujii, 1999) which adopt both ideas of the Lower-Upper Symmetric Alternating Direction Implicit (LU-ADI) and the Lower-Upper Symmetric Gauss-Seidel (LU-SGS). To ensure the time accuracy, backward second order difference formula is used for time integration whereas three sub-iterations (Chakravarthy, 1984) are adopted. The computational time step is 0.003 in non-dimensional time so that the maximum Courant-Friedrichs-Levy (CFL) number becomes approximately 2.0. In the standard LES approach, additional stress and heat flux terms are appended, but in ILES approach (Visbal and Rizzetta, 2002) they are not appended. Instead, a high-order low-pass filter selectively damps only the poorly resolved high-frequency waves. This filtering regularization procedure provides an attractive method to the use of standard sub-grid-scale (SGS) models. Turbulent inflow boundary conditions are generated by using rescaling method of Gerald Urbin *et al.* (2001). Rescaling domain is $-12.0 < x/H < -2.0$. Outflow boundaries are located away from the bump by rapid stretching the mesh in the streamwise direction (Colonius *et al*., 1993). At the outflow boundary, all variables are extrapolated extrapolated from one point front of the outflow boundary. On the lower surface, no-slip conditions are adopted along with a zero normal pressure gradient. Finally, the upper surface is treated as a slip wall ($W = 0$) and the normal derivative of other variables is set to zero. Periodic boundary condition is applied to the spanwise boundaries.

E. Computational grids

Patched grids approach (Fujii, 1995) is employed to generate grids for cavity, orifice, and backward-facing step regions, as shown in Fig. 3, 4 and 5. The grid deformation approach developed by Melville *et al*. (1997) is applied to generate a time-varying fluid grid system for the cavity region. This algebraic method can maintain the grid quality of the initial grid near the deforming surfaces under arbitrary, moderate deflections and rotations. The total number of the grid points is about 7,000,000. (See Table. 1) Between each region, 6 grid points are overlapped to maintain the same accuracy as the internal grid points. The minimum grid size in each direction of all grids is $dx = 0.0017$, $dy = 0.04$ and $dz = 0.0017$, respectively. The length of the computational region in span direction (y-direction) is $4h$. A buffer region is configured (Colonius *et al.*, 1993) to avoid non-physical reflection of acoustic wave as shown in Fig. 3

F. Computational conditions

Inlet flow Mach number and Reynolds number based on height of backward-facing step and free stream velocity are 0.2 and 5000, respectively. 99 percent boundary layer thickness is 1.2*h* at *x/h*=-3.15. Inflow boundary layer is turbulent is boundary layer. Reynolds number and boundary layer thickness are same as those of Jovic' study (1994). Synthetic jet has two important input parameters that are commonly used to describe the operating conditions for flow control; no-dimensional frequency and momentum coefficient. no-dimensional frequency mean frequency of the wall oscillation and no-dimensional momentum coefficient mean ratio of momentum of synthetic jet and free stream.

$$F^{+}_{h} = fh / u_{\infty} \qquad C_{\mu} = \rho u_j^2 d / \rho u_{\infty}^2 h \qquad (2)$$

where f, h, u_∞, ρ , u_j, d and h are the dimensional frequency of the wall oscillation, height of backward-facing step, free stream velocity, density, averaged maximum velocity at orifice exit and width of synthetic jet. The present analysis is focused on the frequency characteristics of the synthetic jet. Three cases are selected, No-control (without synthetic jet), F^{+}_{h} = 0.2 and F^{+}_{h} = 2.0, where non-dimensional frequency F^{+}_{h} is normalized with height of backward-facing step and free stream velocity. Previous studies around airfoil (Amitay *et al.*, 2001; Seifert and Darabi, 1996; Glezer *et al.*, 2005) show that these values are optimal conditions using chord length or separation length as reference length. (See Table 2.) In this study, momentum coefficient use same value (0.2 percent) each cases since the present analysis is focused on the frequency characteristics of the synthetic jet. The value is sufficient small for separation control using synthetic jet. The amplitude use different value of F^{+}_{h} =0.2 and F^{+}_{h} =2.0 because u_j is proportional amplitude and frequency as shown equation (3). (See Table 3.)

$$u_j = k \cdot A \cdot F^{+}_{h} \qquad (3)$$

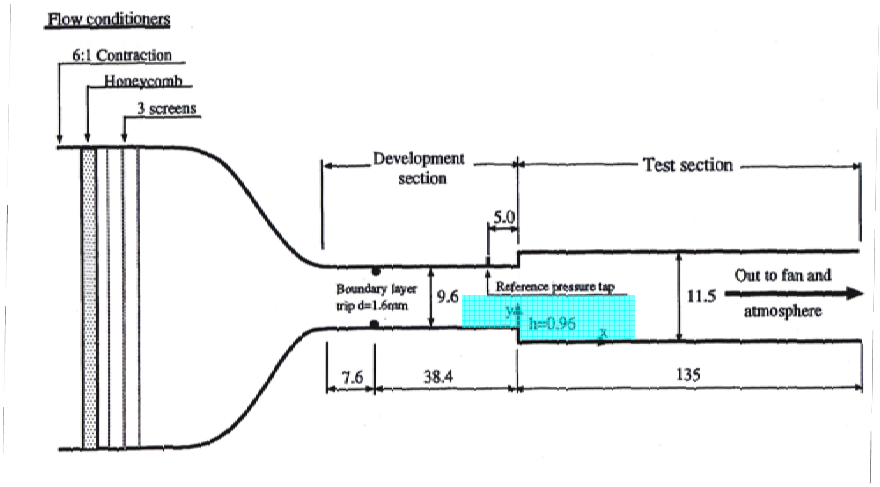

Fig. 2. Wind tunnel schematic(Jovic,1994)

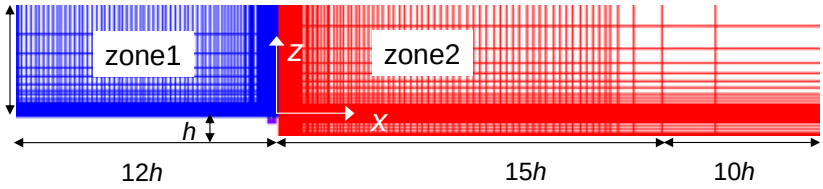

Fig. 3. Computational region

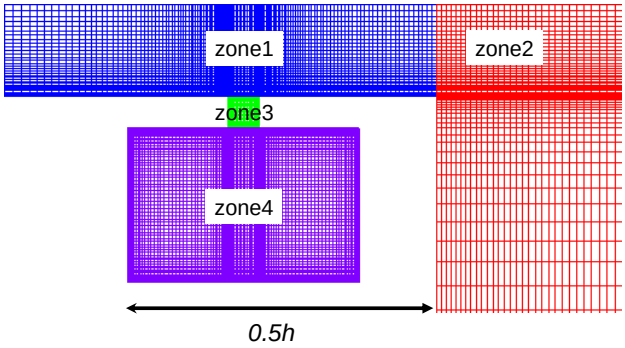

Fig. 4. Cavity grid

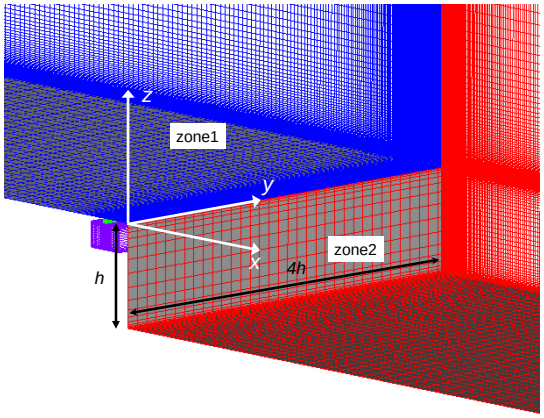

Fig. 5. Computational grid

Table 1. Grid points

zone	name	$j \times k \times l$	$\Delta x/h$	$\Delta y/h$	$\Delta z/h$
zone1	Backstep	349×101× 85	0.0017	0.04	0.0017
zone2	Backstep	268×101×138	0.0027	0.04	0.0017
zone3	orifice	21×101× 43	0.0017	0.04	0.0017
zone4	cavity	99×101× 65	0.0017	0.04	0.0017

Table 2. No-dimensional Frequency

	Backstep		Airfoil	
	F^+_h	F^+_{sep}	F^+_{chord}	F^+_{sep}
Refarence length	Height of Backstep	Length of separation region	Chord length of Airfoil	Length of separation region
	0.2	1.2	1	1
	2	12	10	10

Table 3. Synthetic jet conditions

F^+_h	C_μ	*Amp.*
0.2	0.20%	0.041
2	0.20%	0.0041

RESULTS AND DISSCUSSION

Time averaged flow-fields

Time averaged flow directional velocity and stream line of *y*-constant plane for each three cases are shown in Fig. 6. The stream line means a recirculation region. At No-control case, the flow separate from edge of backward-facing step, configures the recirculation region and reattach the bottom of wall. A small recirculation region also exists after backward-facing step. At $F^+_h = 0.2$, the recirculation region is smaller than No-control case but at $F^+_h = 2.0$, the recirculation region is almost same of No-control case. Fig. 7 show skin frictional coefficient on the bottom wall ($0.0<x/h<10.0$) for each three cases. At $F^+_h = 0.2$, reattached point is obviously shorter than the No-control and $F^+_h = 2.0$. Table 4 mean reattached location calculated form skin frictional coefficient and show that at $F^+_h = 0.2$, length of separation region is shorter 25 percent than the No-control case but at $F^+_h = 2.0$, length of separation region is almost same of No-control case. Fig. 8 shows Reynolds stress distribution for each three cases. At the No-control case, strong Reynolds stress regions exist from the shear layer region ($0.0<x/h<2.0$) and the recirculation region ($2.0<x/h<6.0$). At $F^+_h = 0.2$, the Reynolds stress distribution is wholly high. This enhances mixing of shear layer and separated flow re-attach. At $F^+_h = 2.0$, the Reynolds stress distribution is almost same as the No-control case.

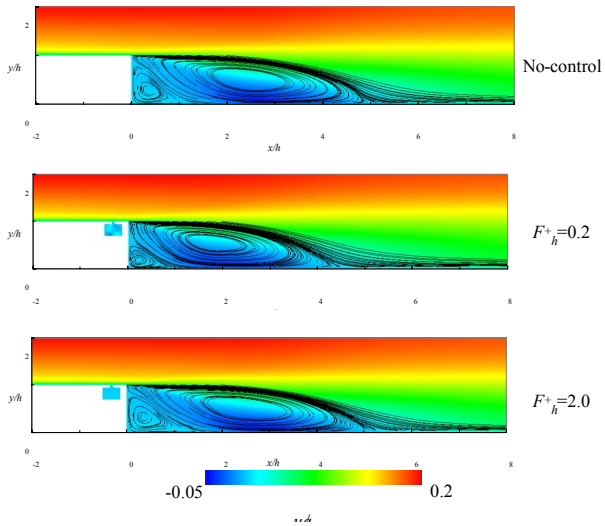

Fig. 6. Flow direction velocity distribution and stream line

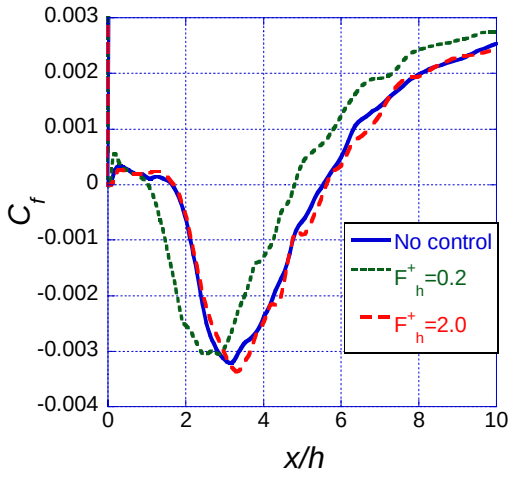

Fig. 7. Skin frictional Coefficient

Table 4. Reattached location

No-control	6.0h
F^+_h=0.2	4.5h
F^+_h=2.0	6.0h

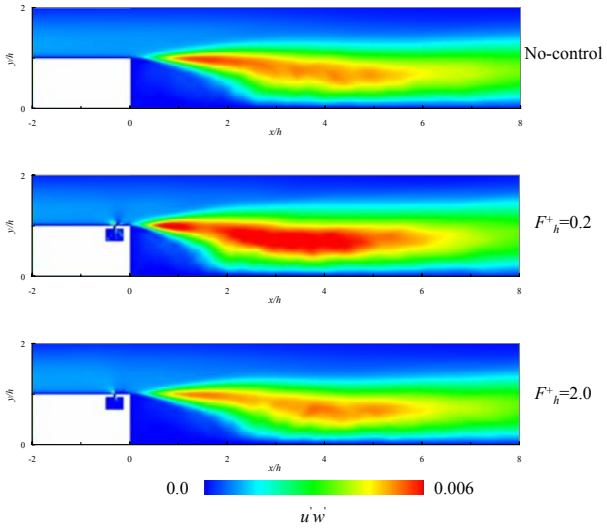

Fig. 8. Reynolds stress distribution

Instantaneous flow-fields

Instantaneous iso-surfaces of the second invariant of the velocity gradient tensor Q and flow directional velocity distribution of each three cases are shown in Fig. 9, Fig. 10 and Fig. 11. Q iso-surface is colored by x-vorticity where red and blue colors respectively show clock-wise and counter-clockwise rotating vortices in the x-direction. This iso-surface indicates vortex structure in general. No-control case, the separated shear layer is induced from the edge of backward-facing step and the vortices are generated in the separated shear layer, then the flow split up and down, the upper flow throw and diffuse after recirculation region. On the other hand, the lower flow counterflow upward, make the recirculation region as shown in Fig. 6 and induce longitudinal vortices in $2.0<x/h<4.0$. At F^+_h =0.2, There are totally a lot of vortices compared with No-control case for synthetic jet blowing. F^+_h =2.0 show more three dimensional flow structure and the strong longitudinal vortices compared with other two cases in $4.0<x/h<8.0$.

Fig. 11, Fig. 12 and Fig. 13 present Instantaneous iso-surfaces of Q and pressure distribution of each three cases. Q iso-surface is colored by y-vorticity where red and blue colors respectively show clock-wise and counter-clockwise rotating vortices in the y-direction. No-control case, vortices are generated in separated shear layer. Moreover, vortices turn to three-dimensional structure in $0.0<x/h<2.0$ by inflow turbulent boundary layer. At F^+_h =0.2, Strong two-dimensional vortices induced from the synthetic jet interact with the shear layer, which results in the increase of the Reynolds stress in the shear layer region. At F^+_h =2.0, Weak and short periodic vortices induced from the synthetic jet because amplitude is small compared with F^+_h =0.2 as shown in Table 3.

Fig. 15, Fig. 16 and Fig. 17 show the time lines of static pressure and 2nd invariant of the velocity gradient tensor Q of each three cases. The Blue lines show same vortex structure. No-control case, vortices are periodically generated in separated shear layer. At F^+_h =0.2, Strong two-dimensional vortices induced from the synthetic jet interact with the shear layer. It seems that F^+_h =0.2 is near shear layer instability frequency of No-control case. These vortices turn to three-dimensional structure, which

possibly make Reynolds stress stronger in the recirculation region. At F^{+}_{h} =2.0, Weak and short periodic vortices induced from the synthetic jet do not interacts with the shear layer very much and diffuse in the recirculation region.

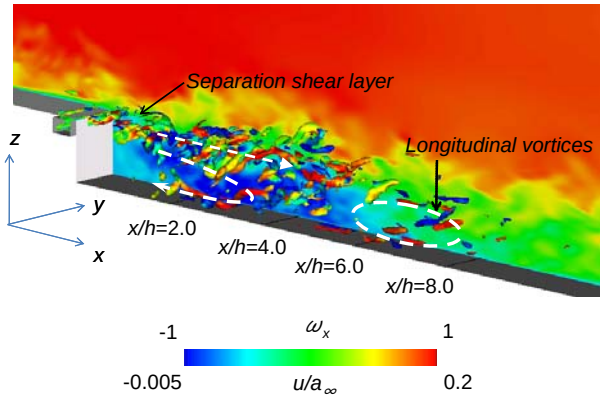

Fig. 9. Iso-surfaces of 2nd invariant of the velocity gradient tensor and Flow direction velocity distribution (Iso-surface is colored by *x*-vorticity), (No-control)

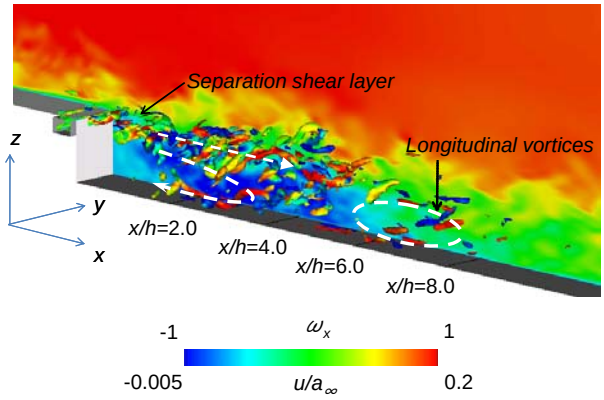

Fig. 10. Iso-surfaces of 2nd invariant of the velocity gradient tensor and Flow direction velocity distribution (Iso-surface is colored by *x*-vorticity), (F^{+}_{h} =0.2)

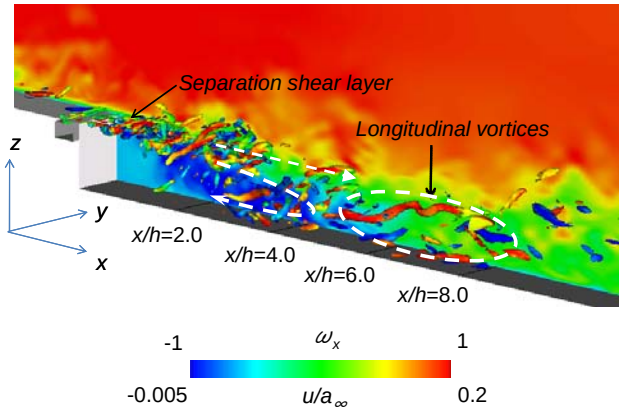

Fig. 11. Iso-surfaces of 2nd invariant of the velocity gradient tensor and Flow direction velocity distribution (Iso-surface is colored by *x*-vorticity), (F^{+}_{h} =2.0)

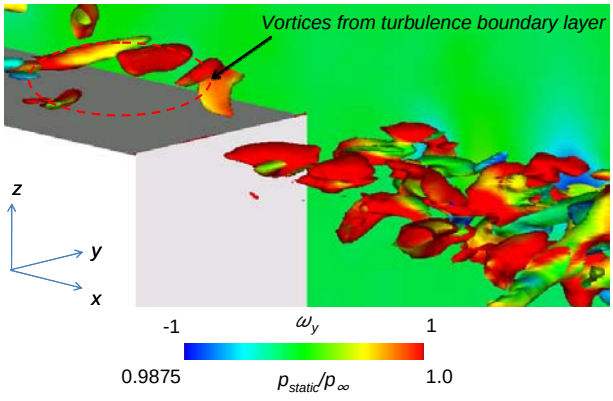

Fig. 12. Iso-surfaces of 2nd invariant of the velocity gradient tensor and Static pressure (Iso-surface is colored by *y*-vorticity), (No-control)

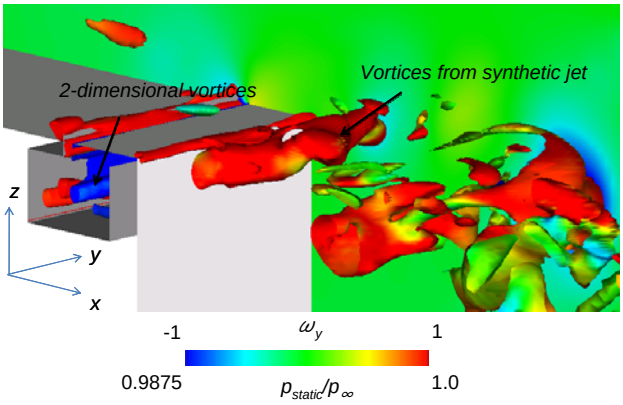

Fig. 13. Iso-surfaces of 2nd invariant of the velocity gradient tensor and Static pressure (Iso-surface is colored by *y*-vorticity), (F^+_h =0.2)

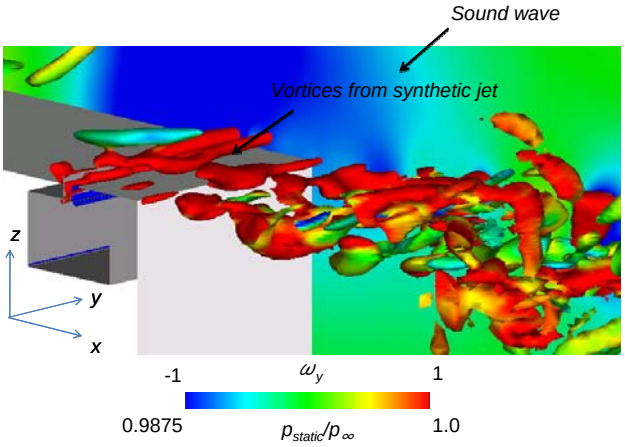

Fig. 14. Iso-surfaces of 2nd invariant of the velocity gradient tensor and Static pressure (Iso-surface is colored by *y*-vorticity), (F^+_h =2.0)

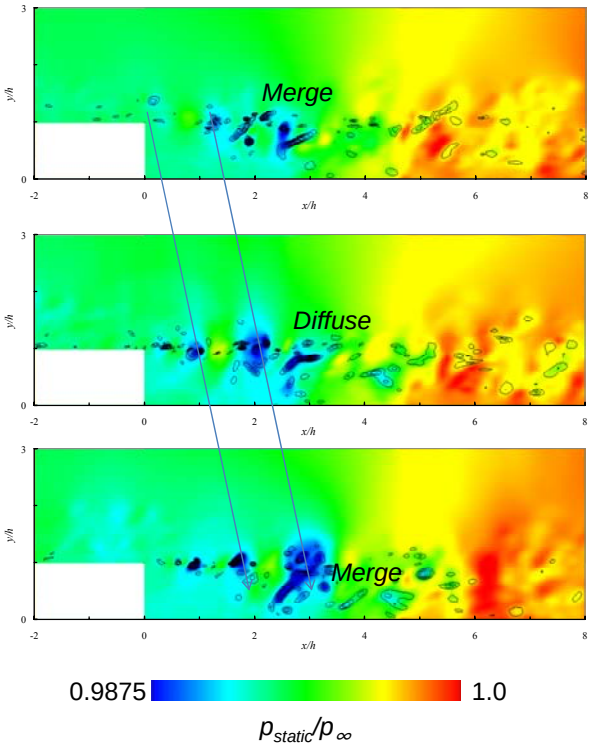

Fig. 15. Static pressure and 2nd invariant of the velocity gradient tensor (black lines, contour range:0.1-3.0 with 20 lines), (No-control)

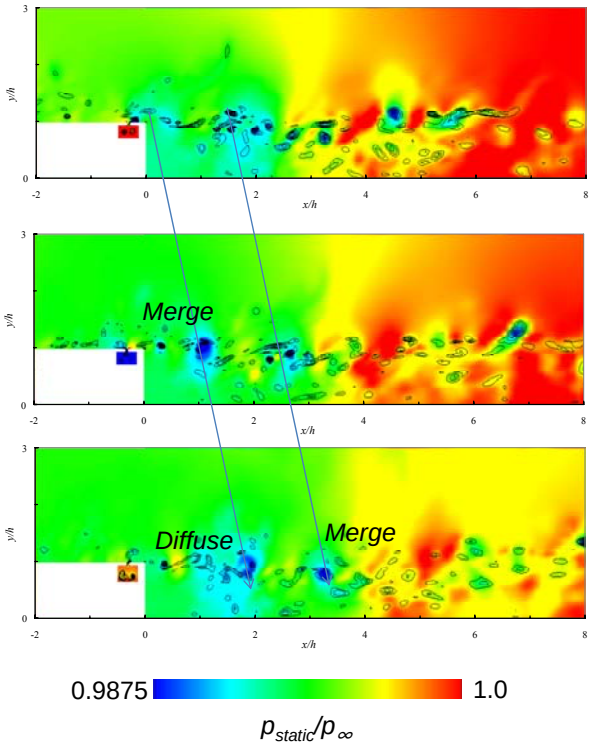

Fig. 16. Static pressure and 2nd invariant of the velocity gradient tensor (black lines, contour range:0.1-3.0 with 20 lines), (F^+_h =0.2)

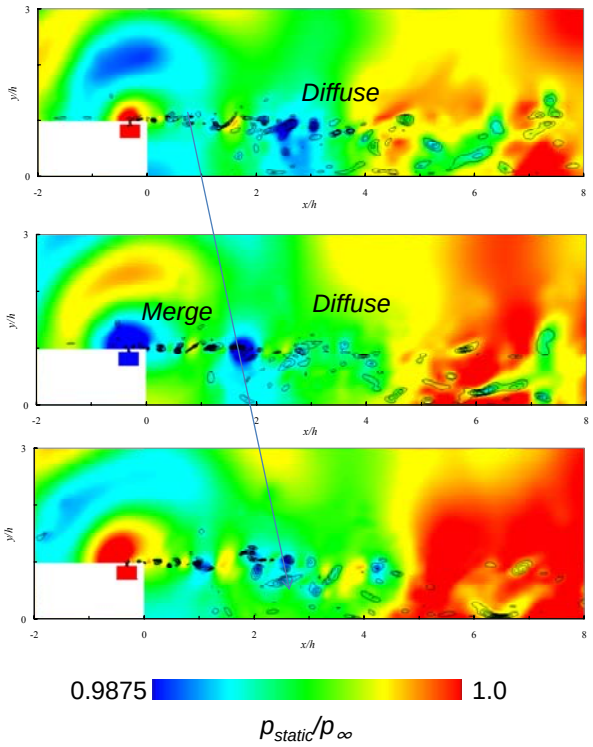

Fig. 17. Static pressure and 2nd invariant of the velocity gradient tensor (black lines, contour range:0.1-3.0 with 20 lines), (F^+_h=2.0)

SUMMARY

The present computation shows that at F^+_h = 0.2, length of separation region is 25 percent shorter than the No-control case. It seems that F^+_h = 0.2 is near shear layer instability frequency of No-control case. Strong two-dimensional vortices induced from the synthetic jet interact with the shear layer, which results in the increase of the Reynolds stress in the shear layer region. These vortices turn to three-dimensional structure, which make Reynolds stress stronger in the recirculation region. At F^+_h = 2.0, length of the separation region is almost same as the No-control case because mixing is not enhanced in the shear layer and recirculation region. Weak and short periodic vortices induced from the synthetic jet do not interacts with the shear layer very much and diffuse in the recirculation region.

REFERENCES

Okada, S. and Hiraoka, K. (2003), "Experimental Studies of Reduction of the Wing Tip Vortex by Suction," AIAA Paper 2003-3533.

Mallinson, H. (1999), "Some Characteristics of Synthetic Jets," AIAA Paper 99-3651.

Amitay, M. *et al.* (2001), "Aerodynamic flow control over an unconventional airfoil using synthetic jet actuators," AIAA Journal, Vol.39, 356-370.

Seifert, A. and Darabi, A. (1996), "Delay of Airfoil Stall by Periodic Excitation," Journal of Aircraft, Vol. 33, 691-699.

Glezer A., Amitay, M. *et al.* (2005), "Aspect of Low-and High-Frequency Actuation for Aerodynamic Flow Control," AIAA Journal, Vol.43, 1501-1511.
Kral, L.D. and Donovan J.F. *et al.* (1999), "Active Flow control Applied to an airfoil," AIAA Paper 98-0210.
Kral, L.D. and Donovan J.F. *et al.* (1997), "Numerical Simulation of Synthetic Jet Actuator," AIAA Paper 97-1824.
Mittal, R. and Ramgunggoon, P. *et al.* (2001), "Interaction of a Synthetic Jet with a Flat Plate Boundary Layer," AIAA Paper 2001-2773.
Okada, K., Fujii, K. and Miyaji, K., (2008), "Effect of Internal Flows in Synthetic Jet Cavity," Fifth International Conference on Computational Fluid Dynamics
Yoshioka, S., Obi, S. and Masuda, S. (2001), "Turbulence Statistics of periodically perturbed separated flow over backward-facing step," International Journal of Heat and Fluid Flow, vol. 22, 393-401.
Rizzetta, D. and Visbal, R.M. (1999), "Numerical Investigation of Synthetic Jet Flowfields," AIAA Journal, Vol.37, No.9, 919-927.
You, D., and Moin, P. (2006), "Larger-eddy simulation of flow separation over an airfoil with synthetic jet control," Center for Turbulence Research Annual Research Briefs.
Srba Jovic (1996), "Backward-Facing Step Measurements at Low Reynolds Number, Reh=5000," NASA TM -08807
Lele, S.K. (1992), "Compact Finite Difference Scheme with Spectral-Like Resolution," Journal of Computational Physics, Vol.103, 16-22.
Gaitonde, D.V. and Visbal, R.M. (2000), "Pade Type Higher-Order Boundary Filters for the Navier-Stokes Equations," AIAA Journal, Vol.38, No.11, 2103-2112.
Visbal, R.M. and Gordnier, R.E. (2000), "Higher-Order Flow Solver for Deforming and Moving Meshes," AIAA Paper 2000-2619.
Fujii, K. (1999), "Efficiency Improvement of Unified Implicit Relaxation/Time Integration Algorithms," AIAA Journal, Vol. 37, No. 1, 125-128.
Chakravarthy, S. R. (1984), "Relaxation Methods for Unfactored Implicit Upwind Schemes," AIAA Paper 84-0165.
M. R. Visbal, and D. P. Rizzetta (2002), "Large-eddy simulation on general geometries using compact differencing and filtering schemes," AIAA Paper 2002-288.
Gerald Urbin and Doyle Knight, (2001) "Large-Eddy Simulation of a Supersonic Boundary Layer Using an Unstructured Grid," AIAA Journal vol.39 No.7, 1288-1295.
Fujii, K. (1995), "Unified Zonal Method Based on the Fortifies Solution Algorithm," Journal of Computational Physics, Vol.118, 92-108.
Melville R. B., Morton S. A. and Rizzetta D. P. (1997), "Implementation of a Fully-Implicit, Aeroelastic Navier-Stokes Solver," AIAA Paper 97-2039.
T, Colonius, S. K. Lele and P. Moin (1993), "Boundary Condition for Direct Computation of Aerodynamics Sound Generation," AIAA Journal, vol. 31, No. 9.